

Fuzzy Logic Based Hysteresis Current Control and Regenerative Braking of BLDC Motor with Battery Equivalent Cell Modelling for Electric Vehicles

Krishna P.S. Praveena , N.S Jayalakshmi[‡] , S. Adarsh 

Department of Electrical and Electronics Engineering, Manipal Institute of Technology, Manipal Academy of Higher Education, Manipal, Karnataka -576104

(praveenakrishna.ps@learner.manipal.edu, jayalakshmi.ns@manipal.edu, adarsh.s@manipal.edu)

[‡]Jayalakshmi N.S., Department of Electrical and Electronics Engineering, Manipal Institute of Technology, Manipal Academy of Higher Education, Manipal, Karnataka -576104, Tel: +91 9481970925, jayalakshmi.ns@manipal.edu

Received: 30.03.2023 Accepted:11.05.2023

Abstract- This article deals with the collective operation of different components of the electric vehicle (EV) including the battery, bidirectional DC-DC converter (BDC), voltage source inverter (VSI), brushless DC motor (BLDCM), and its controller. Temperature modelling and electrical equivalent cell modelling (EECM) of lithium-ion (Li-ion) batteries are particularly important to investigate their performance in real-time. In this research work, the parameters are generated from EECM as a function of both state of charge (SOC) and temperature for a 24V, 15Ah battery pack. Further, the practical battery plant is connected to a 3kW BLDCM drive through mathematically designed BDC and VSI to explore the operation. The VSI switches are operated by the pulses generated through the novel fuzzy logic-based hysteresis current control (FLHCC) to achieve the closed-loop speed control of the drivetrain and regenerative braking (RB) of BLDCM to charge the battery which is not explored in the literature. Though hysteresis current control (HCC) causes higher ripples and less efficiency, it has practical advantages such as simplicity and minimum cost. The system's closed loop operation is examined separately in MATLAB/Simulink with traditional PI controllers and FLC. The results show that FLHCC performs better than the PI controller regarding speed tracking and precision.

Keywords Lithium-ion Battery, electrical equivalent modelling, bidirectional DC-DC converter, brushless DC motor, fuzzy logic-based hysteresis current control, parameter estimation.

1. Introduction

Developing nations like India are usually vulnerable to the issues of pollution, dense population, limited per capita resources, etc. Therefore, the majority of the working class in such countries relies on two-wheeler vehicles for commuting [1]. At present, the trend is shifting towards the electrification of automobiles as a solution to overcome the multi-fold negative consequences of internal combustion engine vehicles such as the emission of greenhouse gases, limited fuel supply, increased fuel prices, and less efficient power conversion [2]. Improvement of the configuration and the performance of the EV drivetrain is critical to realize the commercial viability of EVs. This transformation is possible due to the rapid development in research progress related to battery technology and power electronic circuitry [3, 4].

In EV, the variable load is applied on the motor shaft through the transmission system based on the vehicle dynamics and road conditions [5]. The range of the vehicle depends on energy storage capacity and efficient power conversion including RB of the motor [6]. The selection of a motor for the specific application is based on the main characteristics such as voltage, current, load torque, speed in rpm along with the performance during both steady state and dynamic operating conditions [7]. In addition, capacity, proper sizing, and reliability are critical from the cost point of view [8]. BLDCM is preferred over variable-speed induction motors and synchronous machines due to reduced cost and no additional controllers [7, 9, 10]. PMSM gives better output characteristics, however, for EV applications, the controller is complex and sophisticated [11] increasing the budget. Therefore, for low power capacity within 10kW,

a BLDCM with trapezoidal six-step commutation with simple HCC is quite effective [12].

Bidirectional power flow through BDC and VSI opens the possibility of including RB of the motor which further increases the energy efficiency of the EV drive operation [13]. The constant DC link voltage is regulated through the PI controller in BDC. Similarly, the gating signals to the VSI are generated from the HCC based on the torque reference value produced from the speed controller. This approach is very simple and cost-effective, though it produces ripples in voltage and current waveforms [12, 14]. The other methods like field-oriented control and direct torque control are sophisticated, require complex circuitry and are expensive to implement [14]. PI controllers, the classic approach to regulating the speed of the motor [8], take longer to reach a steady state and fail to effectively manage the varying dynamic load system [15, 16]. Fuzzy logic control is an alternative approach to improve the response time [17]. However, the combination of fuzzy logic and HCC (FLHCC) is not tried so far in the existing literature for the and speed control and the application of RB in low-powered two-wheeler EV drivetrains.

At present, batteries are the primary energy storage utilized in EVs. The battery performance requires a high power-to-weight ratio, high specific energy, energy density, minimum self-discharge, better cycle life, no memory effect, small size, and reduced weight [18]. Although the lithium-ion battery has limitations, it is preferred over other battery technologies [4]. Ultimately, the method of power transfer between the battery and the BLDCM drive decides the overall performance of the complete drive system.

The individual approaches have a good number of merits. The previous works of literature describe the operation of BLDCM with FLC, RB of BLDCM, mathematical EECM of Li-ion batteries, working of BDC, and the drivetrain system of EV with PI controllers separately [13, 17, 18 – 21]. Further, the efforts to develop the complete electric drivetrain for EVs are also available in the literature [22]. However, for the commercial realization of a practical and compact EV at an affordable cost, forming the combination of such different improvisations is important to secure the benefits. This research work focuses on the design and development the drivetrain configuration including the following unique key aspects:

➤ Parameterization and subsequent electrical equivalent cell modelling are developed in the MATLAB/Simulink environment to design a battery pack to realize the real-time dynamic behaviour of the practical battery pack with thermal modelling at different temperatures.

➤ Speed control and regenerative braking of BLDCM driven by the mathematically designed battery pack through the novel combination of the fuzzy logic-based hysteresis current control.

➤ The complete proposed drivetrain of EV is simulated as a pretext to establish the practical operation of the proposed system. Further, PI and fuzzy logic control are applied separately in closed-loop operation for comparison.

After an introduction to the research work, part 2 demonstrates the complete configuration of the designed system, EECM of Li-ion battery, and battery pack design from the parameter estimation technique. Mathematical modelling for closed loop operation of BDC along with the description of VSI is presented in part 3. The mathematical modelling of BLDCM and the speed control concepts including PI control and FLC are narrated in part 4. The MATLAB/Simulink results are exhibited and explained in part 5. Part 6 summarizes the research work based on the design calculations along with the simulation results of the proposed system.

2. Configuration of the Proposed System and the Design of the Battery Pack Using an Electrical Equivalent Cell Model

2.1. Configuration of the Proposed System

In this research procedure, the 24V, 15Ah battery pack is modelled from the cell level using EECM containing one RC pair resembling the practical battery as a function of SOC and temperature. Further, a 48V, 3kW BLDCM load is applied on this equivalent model of battery pack through closed-loop PI-controlled BDC and the VSI regulated by the novel combination of FLHCC to achieve the speed control and RB of the motor drive to charge the battery pack. The DC link voltage at the output of BDC is regulated at 48V through the PI controller. The schematic representation of the proposed system is presented in Fig. 1.

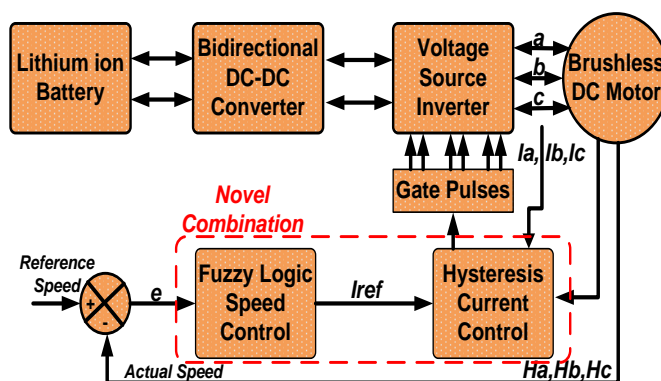


Fig. 1. Block diagram of the proposed drivetrain system

2.2. Battery Equivalent Cell Model

Optimized utilization of Li-ion battery packs including safety and efficiency with improved durability is important in EV applications. This is likely to happen only when the temperature and voltage are maintained within tolerance at cell levels. The available data related to each and every electrochemical phenomenon within a cell is far from precise. In battery status estimation and power control applications, EV designers have adopted lumped-parameter EECM including resistors and capacitors which are responsible for the fidelity of simulation with the behaviour of a real-time operation of battery cell [23]. A single or two RC block cell type with no parasitic branch is a popular choice for lithium cells. Though having a larger number of RC pairs enhances accuracy, it also adds complexity; thus, there is a trade-off to be made when deciding on the number of RC pairs. Fig. 2 shows the one RC equivalent cell model.

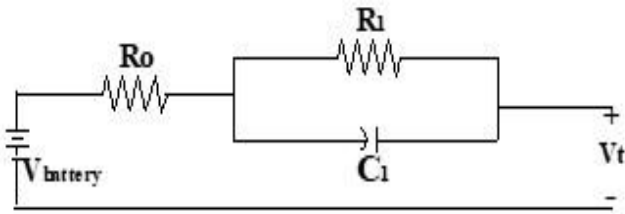


Fig. 2. Equivalent cell circuit with one RC pair [18]

The electrical equivalent model is necessary to obtain the battery voltage as response to the current drawn. V_t or open circuit voltage (OCV) is correlated to the battery SOC to be represented as the ideal voltage of the source. R_0 corresponds to the ohmic resistance offered by the battery cell and the parallel RC network (R_1 and C_1) represents the transient behaviour of the battery resulting from the interfacial charge-transfer reactions at the electrode. The product of R_1 and C_1 represents the time constant for the RC pair [24].

The Thevenin ECM is expressed in discrete form as follows.

$$V_j = OCV - R_0 I_j - U_{1,j} \tag{1}$$

$$U_{1,j+1} = e^{-\frac{\Delta t}{R_1 C_1}} U_{1,j} + [1 - e^{-\frac{\Delta t}{R_1 C_1}}] R_1 I_j \tag{2}$$

where V is the battery terminal voltage, I is the battery current, OCV is the battery open circuit voltage, R_0 is the internal ohmic resistance, U_1 is the voltage of the RC network, R_1 and C_1 are the polarization resistance and capacitance with the product ($R_1 * C_1$) being the time constant of the RC network, and Δt is the sampling time, with the

subscript j being the discrete index. The model parameters OCV , R_0 , R_1 , and C_1 , are known to be functions of SOC and temperature.

The battery parameters depend on the state of charge, temperature, and current [18, 19, 24]. This research work considers SOC and temperature. The ampere-hour counting or coulomb counting is the most extensively used method to calculate the capacity. This method simply integrates current with time to determine the SOC as shown in the following equation.

$$SOC(t) = SOC(t_0) + \frac{\int \eta * I(t)}{C * 3600} \tag{3}$$

Where $I(t)$ is the flow of current into or out of the battery, $SOC(t)$ is determined by the previous SOC (t_0), C is the capacity in Ah and " η " is the columbic efficiency. SOC is usually considered in percentages ranging from 0% to 100%.

2.3. Design of Battery Pack

EV applications demand a battery pack with greater voltage levels, reliability and capacity. To meet the electrical needs of an individual EV system (e.g., the quantity of energy stored, power, voltage range, and maximum current), many battery cells must be combined to form a battery pack [25] involving the cells with similar voltage and capacity. In this research work, parameterized individual EECM with 3.7V, and 2.5Ah ratings are connected in series to obtain 24V, while parallel connections are formed to increase capacity to 15Ah at the battery pack level. The specific voltage and capacity ratings of the battery pack are achieved in such a way that it comprises six parallel modules, each of which contains seven cells connected in series. Thus, a total of 42 cells are connected in series and parallel to form a complete battery pack with a capacity of 24V and 15Ah. The entire battery plant model consisting of the parameter generator block based on the SOC and thermal model block in MATLAB is shown in Fig. 3. OCV , R_0 , R_1 , and C_1 are the parameters selected for one RC network. V_{cell} , I_c , and V_t are the cell voltage, the battery charging current, and the terminal voltages of the battery respectively.

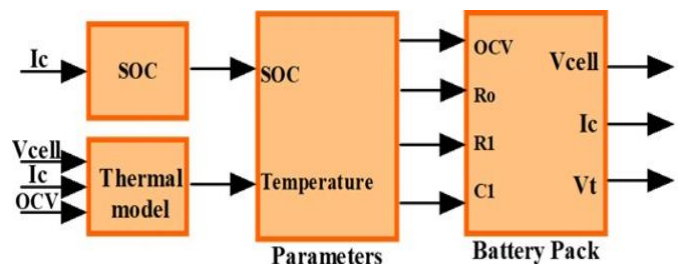


Fig. 3. Complete battery plant model of 24V, 15 Ah

3. Bidirectional DC-DC Converter and Voltage Source Inverter

3.1. Bidirectional DC-DC Converter and Related Equations

In automotive applications, a BDC uses MOSFET/IGBTs to allow the current flow in both directions including motoring of BLDCM to discharge the battery and to charge the battery through RB [13, 20]. Thus, BLDCM can be driven in all four quadrants. The output voltage of BDC is the DC link voltage given to inverter as input. This DC link voltage is regulated by the application of closed loop voltage current controller (PI control). The circuit diagram of the BDC including PI controller is depicted in Fig. 4. The operation of BDC further may be referred from [26].

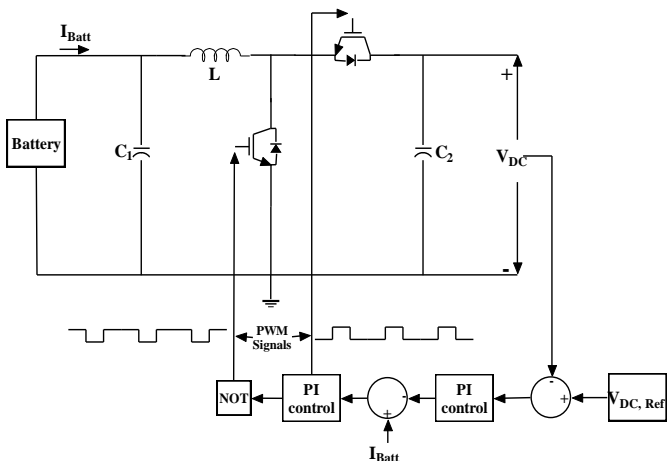


Fig. 4. Circuit diagram of closed loop bidirectional DC-DC converter

The BDC is designed based on the equations given below. Further, the inductor and capacitor specifications are calculated and tabulated in Table 1.

For buck operation:

$$D_1 = \frac{V_{battery}}{V_{bus}} \tag{4}$$

For boost operation:

$$D_2 = \frac{V_{Bus} - V_{battery}}{V_{bus}} \tag{5}$$

Inductor selection:

For buck operation:

$$L_{buck} = \frac{R_1 - (1 - D_1)}{2f_s} \tag{6}$$

For boost operation:

$$L_{boost} = \frac{(1 - D_2)^2 D_2 R_2}{2f_s} \tag{7}$$

Where f_s is the switching frequency, R_1 and R_2 are effective calculated load resistance values.

Output capacitor selection:

For buck operation:

$$C_{buck} = \frac{(1 - D_1)}{8f_s^2 K_{r2} L} \tag{8}$$

For boost operation:

$$C_{boost} = \frac{D_2}{f_s K_{r1} L} \tag{9}$$

K_{r1} and K_{r2} are low and high-voltage side ripple factors.

Table 1. The calculated parameter values of BDC

Parameter name	Symbol	Value	Unit
DC link voltage	V_{bus}	48	V
Battery voltage	$V_{battery}$	24	V
Switching frequency	f_{sw}	20	kHz
Inductance	L	2.4	μH
Capacitance	$C_{battery} = C_1$	6510	μF
Capacitance	$C_{bus} = C_2$	13020	μF
The duty cycle for buck	D_1	0.5	-
The duty cycle for boost	D_2	0.5	-

3.2. Voltage Source Inverter for BLDCM

The three-phase VSI consists of six switches to supply BLDCM. The output signal of the speed controller is modified through the hall sensor six-step signals and then multiplied with torque constant to generate a reference current value. The actual currents are to be compared with the reference current value within the hysteresis band. Thus, the switches of the inverter operate from the gating signals generated from the HCC [14]. The hall sensor rotor position signal is decoded as the exactly needed duty cycle to operate the inverter switches. The pictorial representation of VSI with BLDCM is shown in Fig. 5.

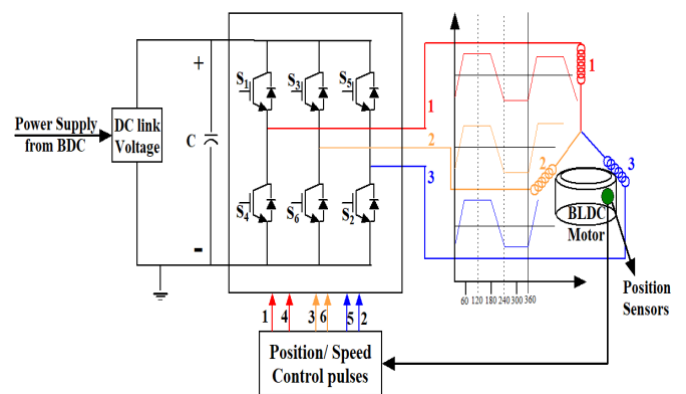


Fig. 5. Six-Step Three Phase Inverter used for BLDCM [14]

4. Mathematical Modelling and Its Control

BLDCM's back EMF is trapezoidal. Therefore, the 'ABC' phase variable model is chosen in this research. A star-connected motor with an isolated neutral is assumed in this model. The analysis was conducted based on the following assumptions.

- The motor is not saturated and run at the rated current.
- All windings have the same stator resistance.
- Both self and mutual inductance are constant.
- Iron and stray losses are insignificant.
- Each of the 3 phases is balanced.
- Uniform air gaps.
- It does not consider hysteresis and eddy current losses.
- Power semiconductor devices used in inverters are ideal.

The mathematical modelling of both the dynamic and steady state of BLDCM is carried out in the form of equations which are referred from [27, 28] for the calculations. The equivalent circuit diagram is depicted in Fig. 6. The calculated specifications of the motor are arranged in Table 2. Three-phase BLDCM with built-in hall sensors was chosen for this project. The rotor position must be detected using hall sensors and fed back into the controller. The reference speed is fed into the controller as input [29].

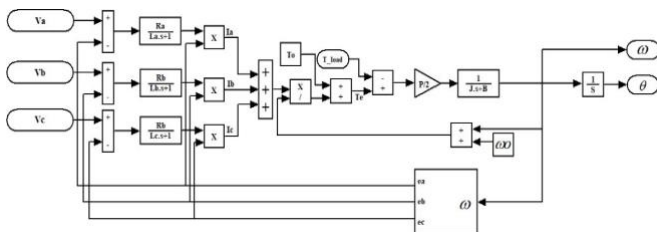


Fig. 6. Schematic of the mathematical model of BLDCM

Table 2. The BLDCM specifications

Parameter name	Symbol	Value	Unit
Pole Pair	p	4	-
Rated voltage	V	48	V
Rated Power	P	3	kW
Rated Speed	N	2000-6000	rpm
Armature Inductance	L_a	68	μH
Armature Resistance	R_a	6.2	$\text{m}\Omega$
Moment of Inertia	J	0.05834	$\text{Kg}\cdot\text{m}^2$
No. of Phases	-	3	-

4.1. Design of fuzzy logic controller

Both in academia and industry, fuzzy logic is gaining prominence because of its ability to emulate human minds with its multi-valued logic that deals with uncertainty and

approximate reasoning [17, 21]. FLC is related to rule-based systems. It is a tool based on language variables that seek to imitate human knowledge of how to regulate systems without using any mathematical models. Depending on the number of linguistic terms used, a fuzzy variable can contain many fuzzy subsets. Each fuzzy subset corresponds to a single linguistic term. The designer selects a variety of shapes to define the fuzzy membership function, such as a triangle, a trapezoid, and so on. The basic structure of the FLC is shown in Fig. 7.

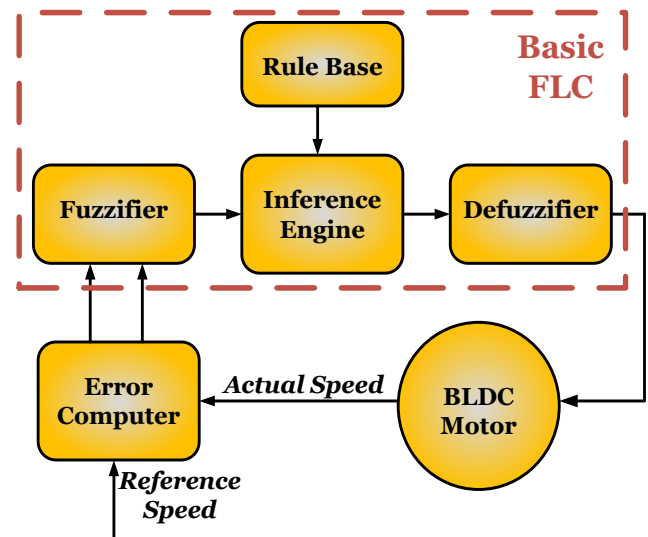


Fig. 7. Structure of a typical Fuzzy Logic Controller [21]

Fuzzification: Fuzzification is the process of transforming a numerical variable into a linguistic/logical variable. Fuzzy variables convert data sources from numerical or crisp values to fuzzy variables, and fuzzy variables are needed for the output. The following language terms are used to quantify the fuzzy variables: error, change in error, and output. Negative Big (NB), Negative Medium (NM), Negative Small (NS), Zero (ZO), Positive Big (PB), Positive Medium (PM), and Positive Small (PS) are the fuzzified values. The membership function for speed error (e), change in speed error (Δe), and the output variable is shown in Fig. 8.

Defuzzification: The centroid method of defuzzification is applied in this research work.

Rule Base and Inference Engine: FLC decides on a choice and generates the control activity using fuzzy principles rather than a numerical equation. The rules created from the rule base are computed using an inference engine. The output of the fuzzy controller is obtained by the evaluation of reporting statuses and behaviour rules. In this approach, there are seven sets of speed errors and changes in speed errors, hence, this fuzzy base has 49 control rules. Table 3 shows the rule base. The MATLAB Fuzzy Logic Toolbox was used to design this rule base.

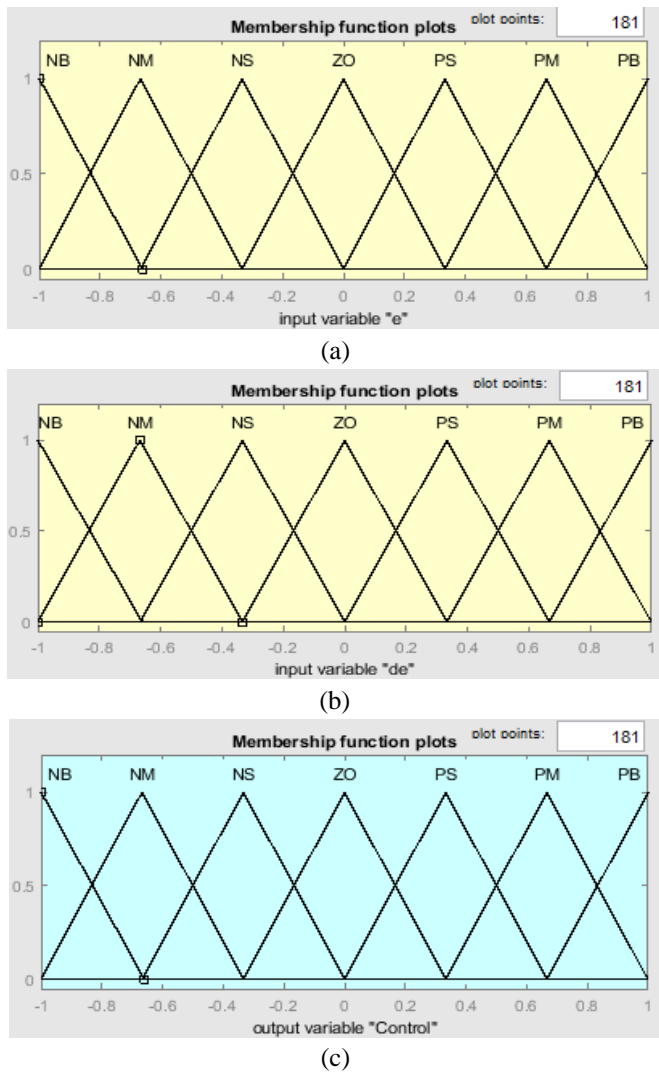


Fig. 8. Membership function of (a) the speed error e (b) change in speed error, Δe (c) output variable

Table 3. Fuzzy rule base

$e/\Delta e$	NB	NM	NS	ZO	PS	PM	PB
NB	NB	NB	NB	NB	NM	NS	ZO
NM	NB	NB	NB	NM	NS	ZO	PS
NS	NB	NB	NM	NS	ZO	PS	PM
ZO	NB	NM	NS	ZO	PS	PM	PB
PS	NM	NS	ZO	PS	PM	PB	PB
PM	NS	ZO	PS	PM	PB	PB	PB
PB	ZO	PS	PM	PB	PB	PB	PB

4.2. Closed loop operation of BLDCM using novel FLHCC Controller

The combination of fuzzy logic and HCC (FLHCC) is not tried so far in the existing literature for the speed control and the application of RB in low-powered two-wheeler EV drivetrains. It is observed that the PI controller is dependent

on the plant model, the current reference produced by the PI controller is not satisfactory in terms of the response time and peak overshoot when the variable load demand is considered. But Fuzzy logic control is independent of the system model. It also compensates for each operating point of the load torque and speed profile. Thus, it gives a better response. When the number of membership functions is more (7 in number), the speed response accuracy is higher. This results in better reference torque values are achieved as shown in Fig. 9. In turn, the current reference signals and the actual signals produce less error to establish better HCC [12].

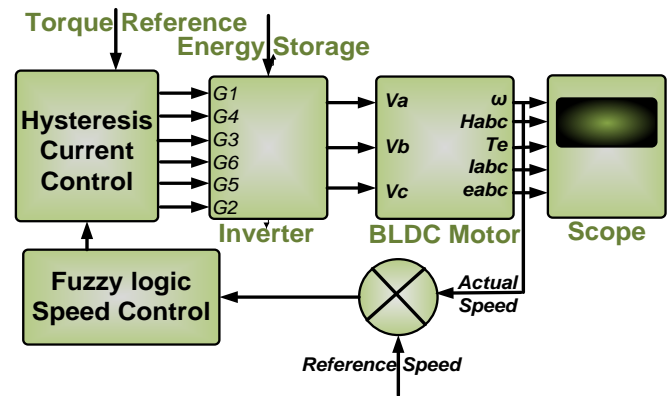


Fig. 9. Schematic diagram of BLDCM with FLHCC control.

Therefore, in this research work, fuzzy logic is applied to control the speed in place of a basic PI control controller. The error signal, which is the difference between the reference and actual speeds, is fed into the speed controller (FLC) to minimize the error in the speed signal. The three-phase inverter powers the BLDCM. The schematic diagram of the BLDCM with novel FLHCC is narrated in Fig. 10.

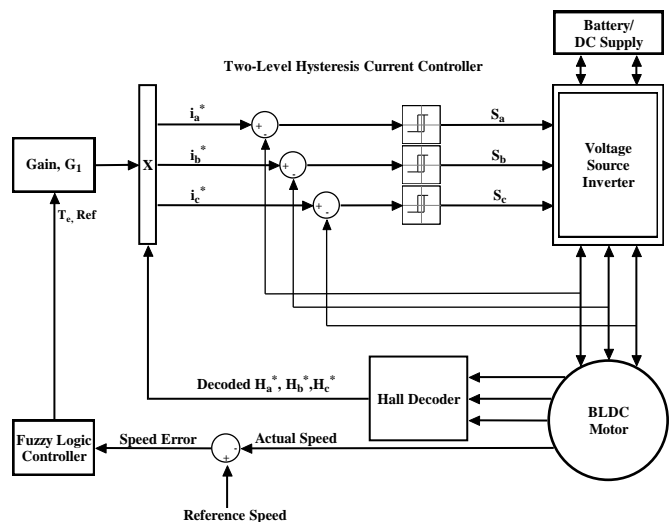


Fig. 10. Detailed narration of the control operation of FLHCC

The torque reference is generated from the fuzzy logic. It is proportional to the three-phase currents. The compensated torque signals are compared with the actual motor torque to get the reference current after dividing with the torque constant. The HCC is also easy to achieve since the three-phase currents are established at the established torque reference value. i_a^* , i_b^* , i_c^* are the reference currents based on the reference torque value T_c . H_a^* , H_b^* , H_c^* are the signals decoded from hall sensors H_a , H_b , H_c . Three two-level hysteresis comparators are used to limit the individual phase currents to generate the switching signals to be given to the inverter switches. These comparators decide the band of the HCC which limits the current values around the reference values. The concept of HCC may be further referred to from [12, 14]. 2% of the motor current is considered as the hysteresis band limit (-0.5 to 0.5) in this research.

5. Results and Discussions

5.1. Parameter estimation of the battery pack

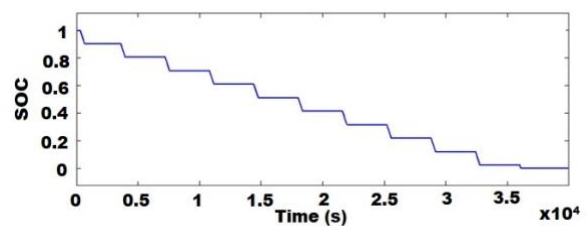
Initially, the parameters OCV, R_0 , R_1 , and C_1 as a function of SOC & temperature are generated in a separate simulation at three different temperatures (i.e., at 5°C, 25°C and 45°C). The variation of OCV is majorly affected by the change in SOC levels but less affected by temperature. Table 4 presents the one RC equivalent circuit data at above mentioned different temperatures. The equivalent circuit parameters were looked up in a set of lookup tables because of this operation. In this study, only pure discharge or charge situations were used, resulting in the polarization of active species in the battery cell. As a result, the fit parameters only reveal discharge relaxation and the effects of polarization hysteresis are ignored.

Table 4. The data of 1-RC equivalent circuit at different temperatures

SOC	Temperature (°C)											
	5°C				25°C				45°C			
	OCV	R0	R1	C1	OCV	R0	R1	C1	OCV	R0	R1	C1
0.1	3.252	0.111	0.0356	9893.7	3.1586	0.0959	0.0103	76375	3.1218	0.0658	0.0125	1518.4
0.2	3.262	0.1059	0.0272	11125	3.2328	0.0931	0.0246	6793	3.2315	0.0758	0.0058	22556
0.3	3.2782	0.1111	0.0187	8920.7	3.2625	0.0952	0.0198	35000	3.2598	0.0808	0.0137	52492
0.4	3.2785	0.1111	0.0249	18759	3.28	0.0936	0.0155	70472	3.284	0.0779	0.0108	143670
0.5	3.282	0.1169	0.0138	7912	3.2898	0.0945	0.0199	26581	3.2935	0.078	0.0126	41221
0.6	3.2892	0.1182	0.0463	7342.2	3.2905	0.0967	0.0166	24086	3.2938	0.0802	0.0078	52145
0.7	3.3268	0.106	0.044	786.56	3.3286	0.1007	0.0266	38256	3.3295	0.0794	0.0466	58391
0.8	3.3285	0.0966	0.0688	1108.1	3.3292	0.106	0.0488	30219	3.3308	0.0868	0.0219	318610
0.9	3.3305	0.1313	0.0953	1608.9	3.3324	0.1018	0.0956	9762.6	3.3312	0.0714	0.9699	11217
1	3.5125	0.2	0.269	1121.8	3.5562	0.1378	0.8782	63.287	3.5806	0.097	1	7.66

5.2. Li-ion cell model

The SOC, current pulse, and cell terminal voltage during discharging of a one RC pair equivalent cell are obtained as shown in Fig. 11 (a-c). The SOC dips at every pulse of current indicating the discharging operation. The discharge current of the battery and the voltage waveforms are presented to show the variation at the moment of the pulse.



(a)

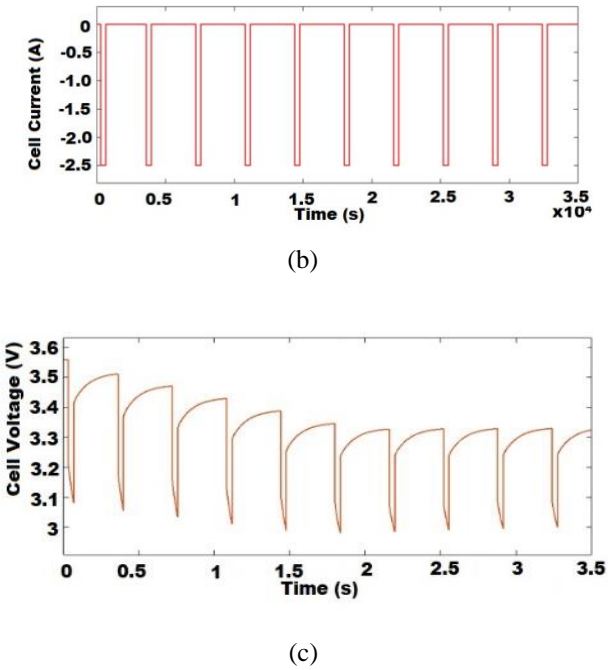


Fig. 11. a) SOC (b) Discharge current (c) Cell Voltage waveforms of one RC pair equivalent cell model

5.3. Battery Pack Model

The battery pack voltage for a given current is shown in Fig. 12 (a), (b). The battery is modelled for a nominal voltage of 24V with a 15Ah capacity.

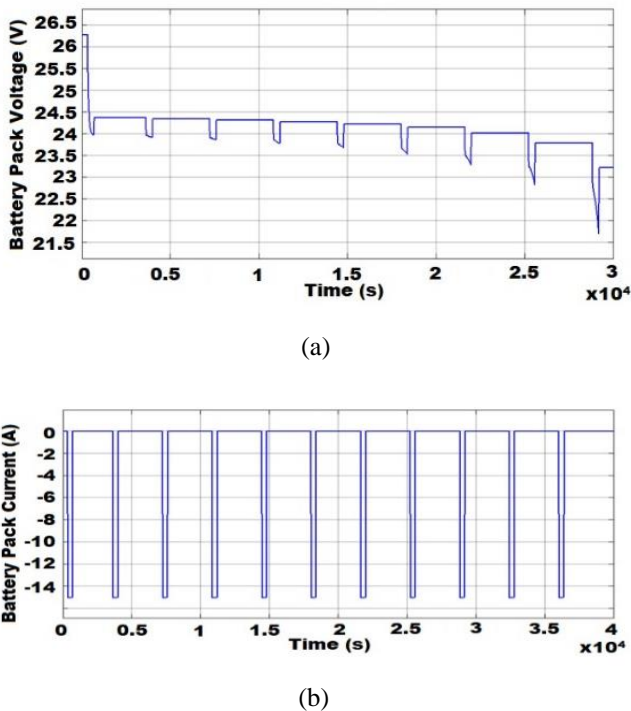


Fig. 12.(a) Voltage and (b) Current waveforms of the battery pack

5.4. Simulation Results of the Proposed System

The MATLAB simulation results are obtained for the speed control and RB of mathematically modelled BLDCM driven by parameterized equivalent battery model through a BDC and VSI. The improvement of the speed response due to the effective application of FLHCC compared to that of PI controller is justified through the following simulation results. All the parameter specification values are calculated for the proposed system from the governing equations of the mathematical models of individual systems. The FIS editor is used to create the fuzzy logic membership functions and rules, which are subsequently exported to MATLAB. The SOC of the Li-ion battery is calculated using the coulomb count method and the Li-ion cell is modelled and simulated using Simulink software for 2.5 seconds. The results are arranged and discussed further.

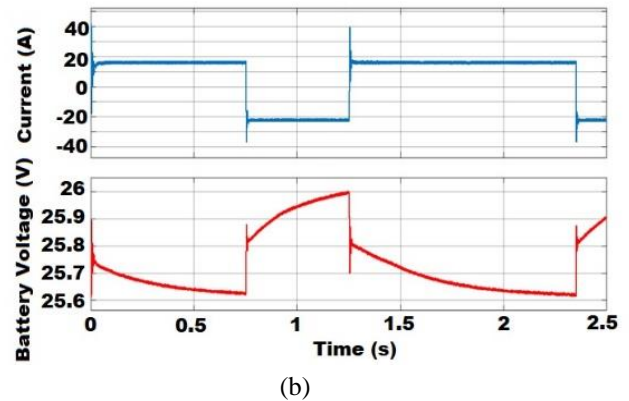
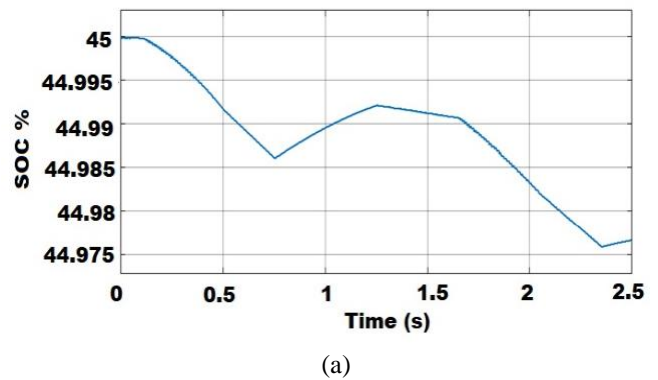


Fig. 13. (a) State of Charge waveform (b) Current and Voltage Waveforms of the battery of the proposed system

Fig. 13 (a) presents the waveform of SOC and Fig. 13 (b) depict the waveform obtained for the time interval of 2.5s respectively. Initially, the battery SOC is kept at 45%. From time 0.05s to 0.65s the SOC is decreasing as it is supplying power to the motor while driving i.e., BLDCM is in the motoring mode of operation. It is observed that the battery current is positive, and the voltage is decreasing because the battery is supplying the power to the load. Now, the converter is in boost mode.

But, from 0.65s to 1.25s the SOC increases because the speed is decreasing at this interval. The battery current is found to be negative during regeneration because the converter is in buck mode, and the battery's SOC begins to increase, as shown in Fig. 13 (a). As a result, the motor functions as a generator, supplying power to the battery. Fig. 13(b) shows the negative battery current and increasing voltage waveforms.

5.5. Fuzzy-based Hysteresis Current Controller for BLDCM

Fig. 14 shows a waveform of FLHCCC-based speed control of the BLDCM including RB. During the first 0.5s of positive speed and torque, the converter switches to boost mode. The BLDCM operates in a normal motoring mode, with power flowing from the battery to the motor. To realize the vehicle's downhill motion, after 0.5s the speed decreases but is still positive. Once the motor provides a negative torque at the time interval of 0.65s, the converter functions in buck mode, recycling electrical energy from the motor to the battery. Later, after 1.25s, for the next 1s, speed goes positive and the motor act as normal. It is seen that the actual speed exactly matches the reference speed with the help of the load independent fuzzy logic controller without any errors or disturbances.

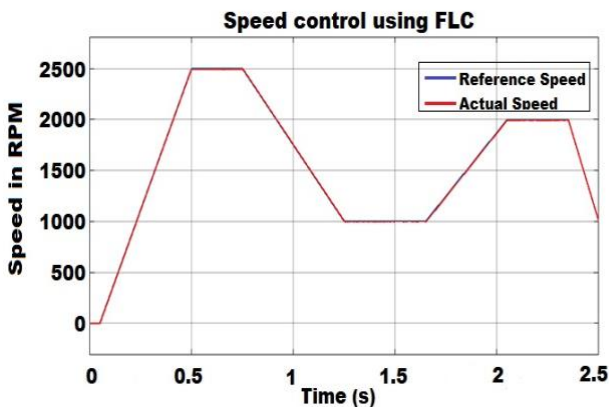


Fig.14. The speed control and RB of the BLDCM using the fuzzy controller

Fig. 15 shows the torque set point values of reference load torque and the electromagnetic torque comparison. From $t = 0$ s to 0.5s, the set point for the speed is 2500 rpm, when the torque supplied to the load is positive, the motor is moving forward in the first quadrant. As demonstrated in Fig. 12, the real speed is exactly following the reference speed with the acceleration ramp. The positive speed set point continues to be maintained when negative load torque is provided to the motor from time $t = 0.75$ s to 1.25s. Real-time speed slows down in order to keep up with the speed set point ramp. There is a braking action in the machine's second quadrant, indicating forward braking. The deceleration of the

rotor speed is shown in Fig. 14. Now, the motor is acting as a generator, at that point. The speed set point and the applied load torque to the motor are both positive for the time $t = 1.65$ s to 2.05s, and the actual speed follows the reference speed.

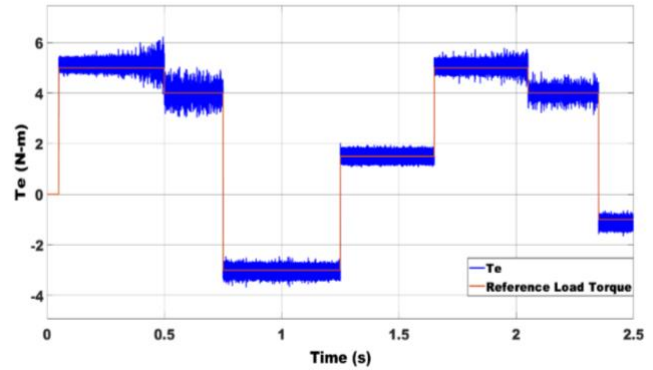


Fig. 15. Reference load torque Vs electromagnetic torque in BLDCM

Fig. 16 shows the three-phase stator current waveforms of a BLDCM, while phase-A, phase-B and phase-C waveforms have the same magnitude but are separated by 120 electrical degrees. It is observed that the waveform is trapezoidal in nature and contains ripples.

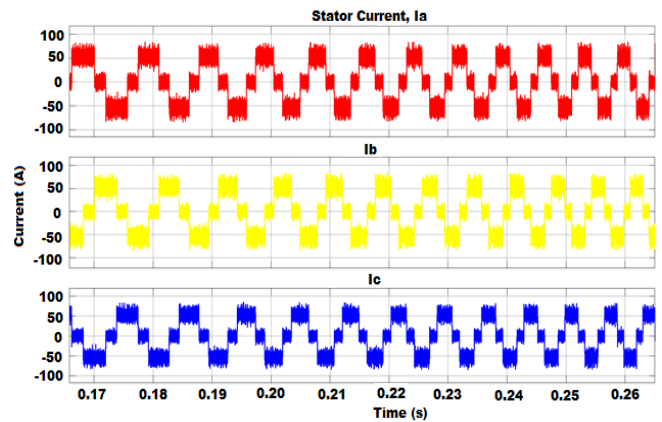


Fig. 16. Three-phase current waveforms given to BLDCM

5.6. Discussions and Comparison of FLHCC with PI controller

Fig. 17 demonstrates the speed response of a BLDCM with a reference speed of 2000 rpm for the novel FLHCC and PI controller for comparison. For a constant load torque of 4 N-m, it is seen that the FLHCC has a faster response. Moreover, the PI controller displays a large peak overshoot. The FLHCC offers a smoother response than the PI controller, with fewer peak overshoots. However, when the load changes, FLHCCC settles for a substantial speed error. The performance of both controllers is given in Table 5.

Table 5. Parameter comparison for PI and fuzzy logic-based hysteresis controllers

Parameter	Controller	
	PI-HCC	FLHCC
Peak overshoot	4.737%	0.505%
Rise time	3.886 ms	.3761 ms

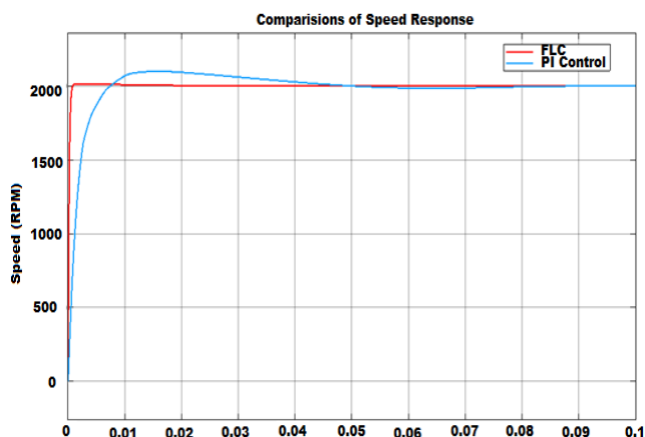


Fig. 17. Comparison of speed control at 2000 rpm for both FLHCC and PI controllers

From Fig. 17, As a speed controller, the FLHCC is better compared to a conventional PI controller. The controller's output is fed into the comparator and then fed into the inverter through HCC. The ripple in the electromagnetic torque's waveform is observed since the trapezoidal nature of the emf and the application of the HCC which is acceptable at low power levels. Hence based on the simulation outcomes, it is inferred that FLHCC is effective in terms of step response and peak overshoot reduction of the speed waveform.

6. Conclusion

In this research work, initially, the electrical equivalent cell model is designed and simulated based on detailed parameter estimation as a function of both SOC and temperature. The influence of temperature is observed. A battery pack of 24V, 15Ah is built using the series and parallel combination of such modelled cells. The results reported for the individual cell and the battery pack are consistent with the data gathered during the literature review. Thus, the battery plant model is considered to be accurate. Further, the proposed drivetrain system is developed consisting of a mathematically modelled 3kW, 48V brushless DC motor driven by the designed battery pack of 24V, 15Ah. Novel combination of fuzzy logic-based hysteresis current control is applied for the speed regulation and regenerative braking of the brushless DC motor drive through voltage source inverter. A separate closed loop bidirectional

converter is employed in the circuitry to increase the source voltage level from 24V and maintain the constant DC link voltage at 48V. The presence of bidirectional converters results in both the charging and discharging of the battery. With or without load, the SOC of the battery decreases during driving and increases during regenerative braking. The performances of both the fuzzy logic-based hysteresis current control and PI controller are evaluated based on different control system characteristics, such as maximum overshoot, and rise time. It is demonstrated that the concept of control using the fuzzy logic-based hysteresis current control has superior speed regulation. Also, the outcome of the application of the fuzzy control is better since there is no overshoot on the speed response and the variations of the torque response are decreased. The design calculations and the simulation results are in good agreement. This implies that the developed system may be subjected to be applied in a real-world setting further.

References

- [1] P. Saraswat, S. V.K., A. Singh, R. Sardar, and S. K. Goel, "Forecasting Penetration of Electric Two-Wheelers in India- Niti Ayog," 2022. [Accessed online on 06/28/2022].
- [2] P. Kamboj, A. Malyan, H. Kaur, and H. Jain, "India Transport Energy Outlook," 2022. (Standards and Reports)
- [3] M. S. H. Lipu, M. Faisal, S. Ansari, M. A. Hannan, T. F. Karim, A. Ayob, A. Hussain, Md. Szal Miah, and M. H. M Saad. "Review of Electric Vehicle Converter Configurations, Control Schemes and Optimizations: Challenges and Suggestions" *Electronics* 10, no. 4: 477. 2021. <https://doi.org/10.3390/electronics10040477> (Article)
- [4] M. Woody, M. Arbabzadeh, G. M. Lewis, G. A. Keoleian, and A. Stefanopoulou, "Strategies to limit degradation and maximize Li-ion battery service lifetime - Critical review and guidance for stakeholders," *Journal of Energy Storage*, vol. 28, no. February, p. 101231, 2020, DOI: 10.1016/j.est.2020.101231. (Article)
- [5] A. Ehsani, M. Gao, Y. Gay, S. E. Emadi, "Modern Electric, Hybrid Electric, and Fuel Cell Vehicles Fundamentals, Theory, and Design," CRC press, 2018. (Book)
- [6] S. Barcellona, D. De Simone, and L. Piegari, "Control strategy to improve EV range by exploiting hybrid storage units," *IET Electrical Systems in Transportation*, vol. 9, no. 4, pp. 237–243, 2019, DOI: 10.1049/it-est.2019.0038. (Article)

- [7] M. Baszynski, "Torque ripple reduction in BLDC motor based on a PWM technique for open-end winding," *Archives of Electrical Engineering*, vol. 70, no. 1, pp. 5–23, 2021, DOI: 10.24425/ae.2021.136049. (Article)
- [8] D. Mohanraj, J. Gopalakrishnan, and B. Chokkalingam, "Critical Aspects of Electric Motor Drive Controllers and Mitigation of Torque Ripple - Review," *IEEE Access*, vol. PP, p. 1, 2022, DOI: 10.1109/ACCESS.2022.3187515. (Article)
- [9] M. Baszyński, "Low cost, high accuracy real-time simulation used for rapid prototyping and testing control algorithms on example of BLDC motor," *Archives of Electrical Engineering*, vol. 65, no. 3, pp. 463–479, 2016, DOI: 10.1515/ae-2016-0034. (Article)
- [10] S. Esmer, and B. Erdal "Design of PMSynRM for Flywheel Energy Storage System in Smart Grids." *International Journal of Smart Grid-ijSmartGrid* 6, no. 4 (2022): 84-91. DOI: 10.20508/ijsmartgrid.v6i4.255.g254 (Article)
- [11] N. Ikram, A. Harrouz, I. Colak, D. Beltrache, V. Dumbrava and K. Kayisli, "Study and Sliding Mode Control of the Permanent Magnet Synchronous Machine," 2022 10th International Conference on Smart Grid (icSmartGrid), Istanbul, Turkey, 2022, pp. 107-110, doi: 10.1109/icSmartGrid55722.2022.9848712. (Conference Paper)
- [12] Y. K. Lee, "Torque Ripple and Switching Power Loss Minimization with Constant Band Hysteresis Current Controller for BLDC Motor," in *Asia-Pacific Power and Energy Engineering Conference, APPEEC, 2019*, vol. 2019-Decem, pp. 1–4, DOI: 10.1109/APPEEC45492.2019.8994737. (Conference Paper)
- [13] X. Nian, F. Peng and H. Zhang, "Regenerative Braking System of Electric Vehicle Driven by Brushless DC Motor," in *IEEE Transactions on Industrial Electronics*, vol. 61, no. 10, pp. 5798-5808, Oct. 2014, DOI: 10.1109/TIE.2014.2300059. (Article)
- [14] J. Zhang, H. Yang, T. Wang, L. Li, D. G. Dorrell, and D. D.-C. Lu, "Field-oriented control based on hysteresis band current controller for a permanent magnet synchronous machine," *IET Power Electronics Research*, vol. 11, no. 7, pp. 1277–1285, 2018. DOI: 10.1049/iet-pel.2017.0651 (Article)
- [15] S. Vadi, F. B. Gurbuz, S. Sagiroglu and R. Bayindir, "Optimization of PI Based Buck-Boost Converter by Particle Swarm Optimization Algorithm," 2021 9th International Conference on Smart Grid (icSmartGrid), Setubal, Portugal, 2021, pp. 295-301, doi: 10.1109/icSmartGrid52357.2021.9551229. (Conference Paper)
- [16] N. Ikram, A. Harrouz, I. Colak, D. Beltrache, V. Dumbrava and K. Kayisli, "Study and Sliding Mode Control of the Permanent Magnet Synchronous Machine," 2022 10th International Conference on Smart Grid (icSmartGrid), Istanbul, Turkey, 2022, pp. 107-110, doi: 10.1109/icSmartGrid55722.2022.9848712. (Conference paper)
- [17] M. Sellali, A. Betka, S. Drid, A. Djerdir, L. Allaoui, and M. Tiar, "Novel control implementation for electric vehicles based on fuzzy -back stepping approach," *Energy*, vol. 178, pp. 644–655, 2019, doi: 10.1016/j.energy.2019.04.146. (Article)
- [18] S. Surya, C. C. Saldanha, and S. Williamson, "Novel Technique for Estimation of Cell Parameters Using MATLAB/Simulink," *Electronics (Switzerland)*, vol. 11, no. 117, 2022, DOI: https://doi.org/10.3390/electronics11010117. (Article)
- [19] S. Hong, M. Kang, H. Park, J. Kim, and J. Baek. 2022. "Real-Time State-of-Charge Estimation Using an Embedded Board for Li-Ion Batteries" *Electronics* 11, no. 13: 2010. DOI: 10.3390/electronics11132010 (Article)
- [20] D. Zhan. "Design Considerations for a Bidirectional DC / DC Converter." *Renesas white paper (September)*:1–9, 2018. (Article)
- [21] O. Guenounou, A. Belkaid, I. Colak, B. Dahhou and F. Chabour, "Optimization of Fuzzy Logic Controller Based Maximum Power Point Tracking Using Hierarchical Genetic Algorithms," 2021 9th International Conference on Smart Grid (icSmartGrid), Setubal, Portugal, 2021, pp. 207-211, doi: 10.1109/icSmartGrid52357.2021.9551249. (Conference Paper)
- [22] G. Thejasree, R. Maniyeri, and P. Kulkarni, "Modeling and Simulation of a Pedelec," 2019 *Innovations in Power and Advanced Computing Technologies, i-PACT 2019*, pp. 1–8, 2019, DOI: 10.1109/i-PACT44901.2019.8960086. (Conference Paper)
- [23] H. Li, W. Zhang, B. Sun, J. Jiang, Z. Yin, J. Wu, and X. He. "Lithium-ion battery modeling under high-frequency ripple current for co-simulation of high-power DC-DC converters." *Journal of Energy Storage* 54 (2022): 105284. DOI: 10.1016/j.est.2022.105284. (Article)
- [24] Q. Wang, T. Gao, and X. Li, "SOC Estimation of Lithium-Ion Battery Based on Equivalent Circuit Model with Variable Parameters," *Energies*, vol. 15, no. 16, pp. 1–15, 2022, DOI: 10.3390/en15165829. (Article)

- [25] F. Chang, F. Roemer, M. Baumann, and M. Lienkamp, "Modelling and evaluation of battery packs with different numbers of paralleled cells," *World Electric Vehicle Journal*, vol. 9, no. 1, 2018, DOI: 10.3390/wevj9010008. (Article)
- [26] H-A. Trinh, D. G. Nguyen, V-D. Phan, T-Q. Duong, H-V-A. Truong, S-J. Choi, and K. K. Ahn. 2023. "Robust Adaptive Control Strategy for a Bidirectional DC-DC Converter Based on Extremum Seeking and Sliding Mode Control" *Sensors* 23, no. 1: 457. <https://doi.org/10.3390/s23010457> (Article)
- [27] N. N. Baharudin and S. M. Ayob, "Brushless DC motor speed control using single input fuzzy PI controller," *International Journal of Power Electronics and Drive Systems*, vol. 9, no. 4, pp. 1952–1966, 2018, DOI: 10.11591/ijpeds.V9n4.pp1952-1966. (Article)
- [28] R. Krishnan. "Electric motor drives: modeling, analysis, and control". Pearson; 2001. (Book)
- [29] G. Shokri and E. Naderi, "Research on simulation and modeling of simple and cost-effective BLDC motor drives," *International Journal of Modelling and Simulation*, vol. 37, no. 1, pp. 15–24, 2017, DOI: 10.1080/02286203.2016.1195665. (Article)
- [27] N. N. Baharudin and S. M. Ayob, "Brushless DC motor speed control using single input fuzzy PI controller," *International Journal of Power Electronics and Drive*